Spatially resolved strain measurements in Mo-alloy micropillars by differential aperture x-ray microscopy

H. Bei,[1,a)] R. I. Barabash,[1,2,b)] G. E. Ice,[1] W. Liu,[3] J. Tischler,[3] and E. P. George[1,4]
[1]*Materials Science and Technology Division, Oak Ridge National Laboratory, Oak Ridge, Tennessee 37831, USA*
[2]*Center for Materials Processing, The University of Tennessee, Knoxville, Tennessee 37996, USA*
[3]*Advanced Photon Source, Argonne, Illinois 60439, USA*
[4]*Materials Science and Engineering Department, The University of Tennessee, Knoxville, Tennessee 37996, USA*

(Received 9 June 2008; accepted 1 August 2008; published online 22 August 2008)

Spatially resolved strain distributions in the NiAl matrix and the ~550–1000 nm Mo fibers of a NiAl–Mo eutectic were investigated by microbeam x-ray diffraction. Position sensitive *d*-spacings for the individual phases were obtained from spatially resolved and energy-resolved Laue patterns. For embedded Mo fibers, the measured elastic strain is consistent with the predicted thermal mismatch strain between the NiAl and Mo phases. However, when the NiAl matrix is etched back to expose Mo micropillars, the *d*-spacing increases to that of unconstrained Mo, indicating release of the compressive residual strain in the Mo fibers. © *2008 American Institute of Physics*.
[DOI: 10.1063/1.2975371]

Recently, single-crystal Mo-alloy micropillars fabricated by directional solidification[1] were shown to deform like defect-free materials and yield at near-theoretical strengths independent of size in the range of 360–1000 nm.[2] This contrasts with the behavior of micropillars fabricated by focused ion beam (FIB) milling, which typically yield at significantly lower stresses and exhibit a size effect (increasing strength with decreasing pillar size).[3] Polychromatic microdiffraction experiments suggest that the deformation behavior of the FIB pillars may be affected by defects introduced during FIB milling.[4] To evaluate the defect state of directionally solidified pillars, we describe here spatially resolved measurements of their elastic and plastic strains. As nanoengineered materials evolve, it will be critical to develop techniques such as this to nondestructively characterize defect distributions at appropriate length scales, and relate the evolving defect distributions to materials behavior.

NiAl–Mo eutectic samples were directionally solidified in high-temperature optical floating-zone furnace at a growth rates of 10 and 40 mm/h. Upon solidification, they organize into well-aligned Mo fibers embedded in a NiAl matrix. The spacing and size of the fibers depend on the growth rate. For this experiment, approximately square cross-section Mo fibers with two different sizes, ~550 nm and ~1 μm, were grown. Details of the directional solidification procedure, and the resulting compositions, microstructures, and orientation relationships can be found in Ref. 1.

Neutron diffraction measurements[5] and calculations[6,7] suggest that stresses develop during solidification between the NiAl and Mo phases because of thermal expansion mismatch. However, the neutron measurements were not conclusive because a reference Mo-alloy single crystal was not available having the same composition as the fibers; therefore, no reference unstrained lattice parameters could be obtained.[5] As discussed before,[1] the composition of the Mo fibers in the directionally solidified NiAl–Mo eutectic is Mo–10Al–4Ni (at. %), which made it impossible to melt a monolithic (single-phase) specimen of this composition because the melting point of Mo is higher than the boiling point of Al resulting in almost complete evaporative loss of Al added as an alloying element.

A direct lattice parameter measurement is, however, possible by x-ray microdiffraction,[8] which can determine the local lattice parameters of submicron crystal volumes. Here, we show how the residual stresses in Mo fibers with submicron dimensions can be measured by differential aperture x-ray microscopy (DAXM).[9–11] This demonstration not only provides important information on the initial state of the Mo fibers, but shows a direct approach to the measurement of residual stresses in composite materials where reference lattice parameters may be difficult to obtain.

Two disk-shaped samples were cut from the directionally solidified NiAl–Mo eutectic rods perpendicular to the growth (fiber) direction and mounted in epoxy. After grinding with SiC paper through 2400 grit they were vibrationally polished, with a slurry of 0.3 μm Al_2O_3 and then with a colloidal suspension of ~20 nm SiO_2. One of the polished

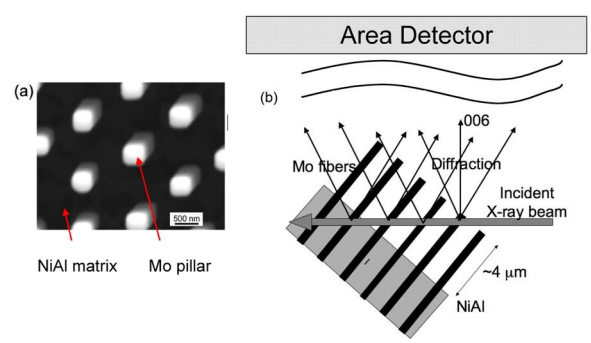

FIG. 1. (Color online) (a) SEM micrograph of fibrous NiAl–Mo eutectic microstructure showing the NiAl matrix etched back to expose Mo-alloy micropillars. (b) Diffraction geometry of NiAl–Mo eutectic samples relative to the incident x-ray beam and detector.

a)Electronic mail: beih@ornl.gov.
b)Electronic mail: barabashr@ornl.gov.

 © 2008 American Institute of Physics

Downloaded 06 Sep 2009 to 160.91.157.167. Redistribution subject to AIP license or copyright; see http://apl.aip.org/apl/copyright.jsp

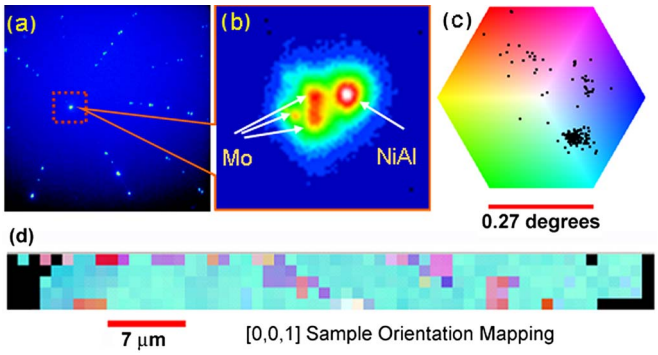

FIG. 2. (Color online) (a) Typical Laue pattern from NiAl–Mo eutectic sample. (b) Magnified central (006) reflection showing Laue spots from the NiAl matrix and multiple Mo fibers. (c) Orientation spread around the Mo [001] surface normal. (d) Sample orientation map around the [001] direction. Note the spread in Mo peaks due to the small (<0.27°) misorientations of the Mo fibers; typically several (up to 10) different Mo fibers are intercepted by the beam at different depths below the surface along the beam penetration trajectory.

samples was immersed in a water solution containing 18% HCl and 8% H_2O_2 to etch away ~4 μm of the NiAl matrix to produce a surface with exposed Mo-alloy fibers.

Both polychromatic and monochromatic x-ray microdiffraction were used to characterize the two samples, with a diffraction geometry shown schematically in Fig. 1(b). A focused (~0.5 μm diameter) x-ray beam intersects at 45° to the sample surfaces, which is normal to the fiber axis and crystallographic [001] normal for both the NiAl and Mo phases. The diffraction patterns were recorded with a charge-coupled device detector located at 90° to the incident beam [Fig. 1(b)]. As described in Ref. 10, the deviatoric and absolute elastic strain tensors can be determined from polychromatic and monochromatic measurements of the diffraction. In addition, the depth-resolved strains can be determined using DAXM.[9–11]

As an initial step, the overall alignment of the fibers and single-crystal matrix were studied with polychromatic microdiffraction. With a small (~0.5 μm diameter) polychromatic beam incident on the sample, a characteristic Laue pattern is generated as shown in Fig. 2(a). This Laue pattern is a superposition of Laue patterns from the NiAl matrix and the Mo fibers. An enlarged image of the central [006] Laue spot is shown in Fig. 2(b). As the orientations of the matrix and fibers are similar, each Laue spot consists of two subpeaks belonging to NiAl and Mo [Fig. 2(b)]. Generally, streaking in the Laue pattern indicates the presence of elastic strain gradients, geometrically necessary dislocations, or can arise from extended diffraction through a thick sample. For these samples, negligible streaking was observed in the Mo peaks indicating the absence of these features.

To further characterize the sample, variations in the local alignment of the Mo fibers were studied by mapping the distribution of fiber orientations over a 5×50 μm^2 area. A pole figure and two-dimensional sample orientation map are shown in Figs. 2(c) and 2(d). There is a small orientation spread of the Mo fibers ($<\sim 0.27°$) around the [001] direction but no clear spatial correlation is observed in the orientation distribution.

The depth-resolved (006) d-spacing distribution was measured with an energy-scan method. Here the diffraction near a Laue reflection is observed as a function of a scanned

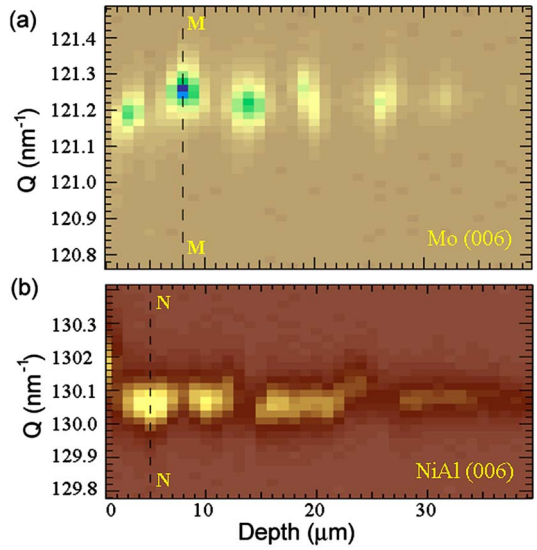

FIG. 3. (Color online) Inverse lattice parameters obtained from the (006) reflections for the NiAl–Mo composite (~1 μm fibers) as a function of depth below the polished surface: (a) Mo fibers and (b) NiAl matrix. Dashed lines MM and NN indicate positions of maximum intensity for Mo (MM) and NiAl (NN) Laue spots. Note that the locations of maximum intensity for Mo and NiAl alternate, consistent with the alternating fiber-matrix arrangement shown in Fig. 1(b).

incident beam energy.[10,11] The energy was scanned in 2 eV steps over a range of ~140 eV. The exact scan range varied from point to point due to the small (up to ~0.27°) misalignment of the Mo fibers. The spatially resolved d-spacings of the NiAl matrix and Mo fibers are shown in Fig. 3, which presents inverse d-spacing measurements as a function of depth of the (006) diffraction vector, Q, with modulus $|Q| = 2\pi/d$ for the as-polished NiAl–Mo composite containing embedded (i.e., nonexposed) fibers. In this state, both the Mo fibers and NiAl matrix show d-spacing ($2\pi/Q$ in Fig. 3) variations of ~0.1%, indicating that there may be slight compositional and/or elastic strain variations along the fiber direction.

Compared to the as-polished sample, which contains Mo-alloys fibers embedded in the NiAl matrix, the etched sample, which has ~4 μm long Mo-alloy pillars sticking out of the surface, is significantly different. Figure 4 shows the d-spacing variation for the exposed pillars as a function

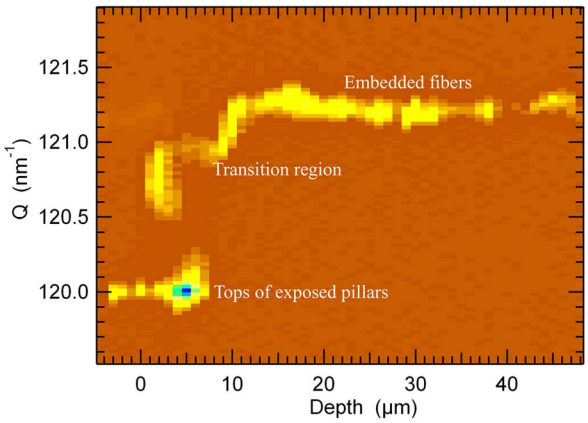

FIG. 4. (Color online) Inverse lattice parameters obtained from the (006) reflections as a function of distance along the fiber axis from the tops of the exposed ~550 nm Mo-alloy micropillars. The d spacing in the exposed pillars is ~1% larger than that in the embedded fibers.

Downloaded 06 Sep 2009 to 160.91.157.167. Redistribution subject to AIP license or copyright; see http://apl.aip.org/apl/copyright.jsp

of distance from the NiAl surface. Above the surface, the d-spacings increase by $\sim 1.0\%$. Below the surface, the d-spacings are similar to those shown in Fig. 3 for the as-polished sample containing embedded fibers. In other words, the Mo fibers have a smaller lattice parameter (i.e., they are in compression) when they are embedded in the NiAl matrix and relax when the matrix is etched back. In contrast, the NiAl matrix in the composite has a larger lattice parameter (i.e., is in tension) compared to a monolithic single crystal of the same composition and orientation.[5] Interestingly, the relaxed lattice parameter of the Mo-alloy pillars approaches that of pure Mo even though the former are known to contain 4 at. % Ni and 10 at. % Al based on microprobe analysis.[1]

The above results can be compared with those expected from thermal expansion mismatch between the Mo-alloy fibers and the NiAl matrix during directional solidification from the melt. In general, the magnitude of the thermal residual stress along the fiber direction is a function of the volume fraction of the fiber, difference in coefficients of thermal expansion (CTEs), temperature change, elastic constants, and other mechanical properties of the two phases. To calculate this stress, and model the elastic strain, one should take into account the fact that the fibers are surrounded by the matrix and use, for example, an axisymmetric model[12] to obtain an exact solution. However, for continuous-fiber-reinforced composites, the difference between the results obtained using axisymmetric and one-dimensional models is small.[12] Since our Mo fibers have long aspect ratios (>200), it is reasonable here to make the continuous-fiber approximation and use a one-dimensional model. Although, strictly speaking, our geometry is not axisymmetric (our fibers have square rather than circular cross sections); the uncertainties in the anisotropic elastic constants are too large to justify more exact model calculation. Furthermore, upon heating, the matrix and fiber in this NiAl–Mo system coexpand along the fiber axis but expand independently in directions perpendicular to the fiber direction, as shown by neutron diffraction.[5] Therefore, the residual elastic strain (ε) in the fibers may be estimated using a one-dimensional model:

$$\varepsilon = \Delta\alpha\Delta T,$$

where $\Delta\alpha$ is the difference in the axial CTEs of the fibers with and without the matrix and ΔT is the change in temperature. Since the CTE difference is 8×10^{-6} K^{-1},[5] and the temperature difference between the melting point of the NiAl–Mo eutectic (1600 °C) and room temperature (25 °C) is 1575 °C, the compressive strain in the fibers should be 1.3%. This value is larger than the measured strain in the embedded fibers and likely an overestimate because, at 800 °C, the NiAl matrix yields plastically and is unable to sustain any elastic strain.[5] That is, the ΔT in the above equation should not be based on the melting point but rather on some lower temperature where the NiAl matrix is able to elastically constrain the fibers. If we choose the ductile-brittle transition point ($\sim$750 °C) as this temperature, then ΔT should be $750-25=725$ °C, and the calculated mismatch strain becomes 0.6%. Since the measured strain ($\sim 1\%$) lies between the above two limiting cases (1.3 and 0.6%), it suggests that elastic constraint from the NiAl matrix becomes effective at some temperature below the melting point but above the ductile-brittle transition point. Transmission electron microscopy has shown that dislocations are present in the NiAl phase of the as-solidified NiAl–Mo eutectic, but not in the Mo fibers, suggesting that only the NiAl phase yields plastically at elevated temperatures.[13]

In conclusion, microbeam x-ray diffraction was applied to investigate the depth dependent spatial distributions of the d-spacings of Mo-alloy pillars as small as $\sim$550 nm in diameter. It is found that the d-spacings of exposed Mo-alloy pillars are $\sim 1\%$ larger than those of Mo-alloy fibers embedded in a NiAl matrix. The thermal residual strain resulting from the CTE mismatch between Mo and NiAl causes the embedded fibers to be in compression. When the NiAl matrix is etched back this mismatch strain is released resulting in a larger d spacing in the Mo-alloy micropillars. This experiment demonstrates the applicability of local diffraction methods to nanoengineered materials, and illustrates an approach for studies of local elastic strain distributions in composite materials where reference lattice parameters may be difficult to obtain.

This research was sponsored by the Division of Materials Sciences and Engineering, U.S. Department of Energy. Data collection with PXM was carried out on beamline ID-34-E at the Advanced Photon Source, Argonne IL, which is supported by the Office of Basic Energy Sciences, U.S. Department of Energy, under Contract No. W-31-109-ENG-38.

[1] H. Bei and E. P. George, Acta Mater. **53**, 69 (2005).
[2] H. Bei, S. Shim, E. P. George, M. K. Miller, E. G. Herbert, and G. M. Pharr, Scr. Mater. **57**, 397 (2007).
[3] For example, M. D. Uchic, D. M. Dimiduk, J. N. Florando, and W. D. Nix, Science **305**, 986 (2004).
[4] R. Maaß, S. Van Petegem, H. Van Swygenhoven, and P. M. Derlet, Phys. Rev. Lett. **99**, 145505 (2007).
[5] H. Bei, E. P. George, D. W. Brown, G. M. Pharr, H. Choo, W. D. Porter, and M. A. M. Bourke, J. Appl. Phys. **97**, 123503 (2005).
[6] A. Misra, Z. L. Wu, M. T. Kush, and R. Gibala, Mater. Sci. Eng., A **239**, 75 (1997).
[7] H. Bei, E. P. George, and G. M. Pharr, Mater. Sci. Eng., A **483**, 218 (2008).
[8] J.-S. Chung and G. E. Ice, J. Appl. Phys. **86**, 5249 (1999).
[9] B. C. Larson, W. Yang, G. E. Ice, J. D. Budai, and J. Z. Tischler, Nature (London) **415**, 887 (2002).
[10] W. Yang, B. C. Larson, J. Z. Tischler, G. E. Ice, J. D. Budai, and W. Liu, Micron **35**, 431 (2004).
[11] G. E. Ice and R. I. Barabash, *White Beam MicroDiffraction and Dislocations Gradients*, Dislocations in Solids Vol. 13, edited by F. R. N. Nabarro and J. P. Hirth (Elsevier, New York, 2007), pp. 500–601, Chap. 79.
[12] H. Zhang, P. M. Anderson, and G. S. Daehn, Metall. Trans. A **25**, 415 (1994).
[13] A. Misra, Z. L. Wu, M. T. Kush, and R. Gibala, Philos. Mag. A **78**, 533 (1998).

Downloaded 06 Sep 2009 to 160.91.157.167. Redistribution subject to AIP license or copyright; see http://apl.aip.org/apl/copyright.jsp